PHYSICS OF CORONAL MASS EJECTIONS: A NEW PARADIGM OF SOLAR ERUPTIONS

JAMES CHEN
Plasma Physics Division, Naval Research Laboratory

Abstract. The prevailing framework of understanding coronal mass ejections (CMEs) and, indeed, solar eruptions in general is the hypothesis that the quasi-static changes in the photospheric magnetic field increases the magnetic energy in the corona and causes sudden release of the stored energy. However, this hypothesis, which may be called the 'storage-release' paradigm, has yet to produce a quantitative model of CMEs and their heliospheric consequences. Recently, a new theory has been proposed to explain the physics of CMEs. This theory posits that the initial structure is a magnetic flux rope that is ultimately connected to the solar dynamo in the convection zone and that magnetic energy propagating from the source along the submerged magnetic structure enters the corona and drives the eruption. Specifically, the theory describes CMEs as the dynamical response of coronal flux ropes to the 'injected' poloidal flux and predicts that CMEs evolve into interplanetary magnetic clouds (MCs). In a recent series of studies, the physics-based theory was shown to correctly describe the observed dynamics of a class of CMEs and the properties of MCs, providing the first unified description of the CME-MC dynamics. The apparent success of the theory suggests a new paradigm in which CMEs are viewed as a relaxation process in response to the increased magnetic energy propagating from the dynamo. The motion of a flux rope and its magnetic energy is everywhere given by $\tilde{v} \lesssim 1$, where $\tilde{v} \equiv v/V_M$ and V_M is the local characteristic speed. It is predicted that the injected poloidal flux can cause a subtle but distinct signature in the tangential field at the base of the corona. The tangential field, which is difficult to observe, and the poloidal magnetic energy have been neglected in previous theories. This paper reviews the current CME research, compares the physics of the two competing paradigms, and suggests new observable magnetic field signatures.

Introduction

The Sun has fascinated mankind for centuries and has been an object of attention from time immemorial. The existence of sunspots has been known for over 2000 years. Drawings of sunspots date back to the 17th century, and prominences have been noted during eclipses for hundreds of years. Solar flares were first seen in white light in 1859 using telescopes on the ground (Carrington, 1860; Hodgson, 1860). A century later, a new eruptive phenomenon was discovered by satellite observations, now referred to as coronal mass ejection (CME). They were first observed by the coronagraph on Orbiting Solar Observatory 7 (OSO-7) (Tousey, 1973). Subsequently, they were observed by *Skylab* (MacQueen *et al.*, 1974; Gosling *et al.*, 1974), the Solwind coronagraph on the P78-1 satellite (Michels *et al.*, 1980; Sheeley *et al.*, 1982; Howard *et al.*, 1985), and the Solar Maximum Mission (SMM) satellite (MacQueen *et al.*, 1980). Since 1996, the Large Angle and

Space Science Reviews **95:** 165–190, 2001.

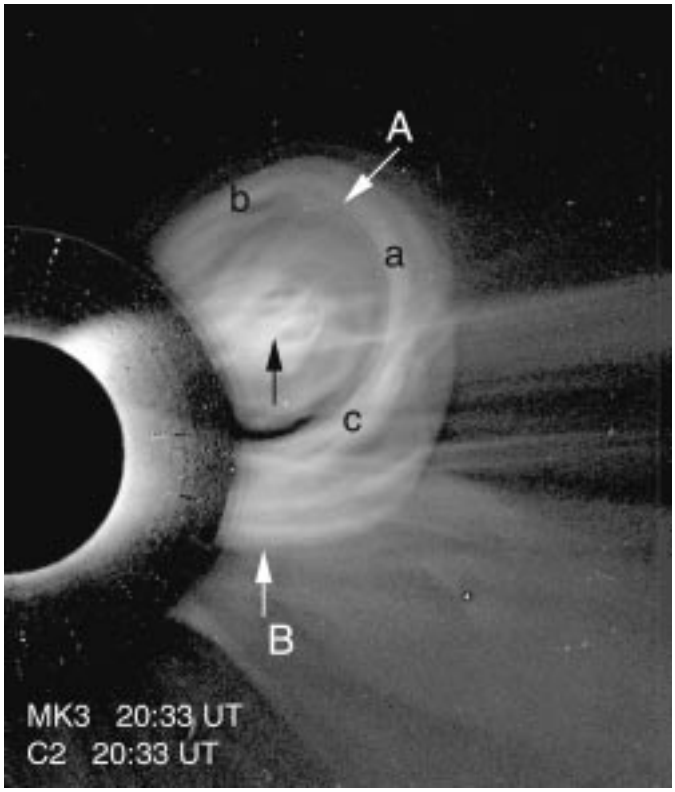

Figure 1. Fast (∼900 km/s) CME of 1997 September 9. Composite of MK3 (inner image) and LASCO/C2 (outer image) data matched at ∼2.2 $R_\odot$. *A* and *B* mark the bright rim and its southern extension. The leading edge and the top and the bottom edges are marked by *a*, *b*, and *c*, respectively. From *Chen et al.* (2000).

Spectrometric Coronagraph (LASCO) on the Solar and Heliospheric Observatory (SOHO) satellite has recorded nearly a thousand CMEs. The LASCO instrument (Brueckner *et al.*, 1995) has a Sun-centered field of view of 32 solar radii ($R_\odot$) and with its high dynamic range and sensitivity, provides an unprecedented view of the solar corona three to four times wider than previous coronagraphs. Indeed, due to the International Solar Terrestrial Physics (ISTP) program, the empirical understanding of CMEs and their heliospheric consequences has improved dramatically in the last decade.

In coronagraph observations, CMEs appear as bright features, generally having spatial scales of the order of a solar radius ($R_\odot$) and expanding outward at speeds of up to ∼2000 km/s, with the average projected speed of about 400 km s^{-1} (Gosling *et al.*, 1974; Howard *et al.*, 1985; Hundhausen *et al.*, 1994; St. Cyr *et al.*, 1999). Figure 1 shows a CME recently observed by LASCO and the ground-based Mauna Loa Solar Observatory Mark III (MK3) K-coronameter (Fisher *et al.*, 1981). (A detailed study of this event has been reported elsewhere (Chen *et al.*, 2000).) The

black semi-circle on the left is the western half of the MK3 occulting disk (radius 1.1 $R_\odot$). The inner image is the MK3 channel 0 data (1.1 $R_\odot$ to 2.4 $R_\odot$). The outer image was obtained by the LASCO C2 coronagraph (a field of view of 2–6 $R_\odot$). In the C2 image, we see a bright loop-like rim *A* with a southern extension indicated by arrow *B*. The leading edge (a) and the top (b) and the lower (c) edges of rim *A* are marked. An arrow points to the 'core' of the cavity, presumed to be an eruptive prominence. CMEs such as this can maintain their apparent structural integrity through the LASCO field of view. This suggests that they are organized by magnetic field.

In interplanetary space, a class of solar wind (SW) structures, referred to as magnetic clouds (MCs) first discovered by Burlaga *et al.* (1981), have been closely associated with CMEs (e.g., Wilson and Hildner, 1984; Burlaga *et al.*, 1998; Webb *et al.*, 2000). Although the evolutionary connection between CMEs and MCs has not been directly observed, there is strong observational (Larson *et al.*, 1997) and theoretical (Chen and Garren, 1993) evidence that MCs are flux ropes with their magnetic fields ('legs') connected to the Sun.

Although solar flares were long thought to cause geomagnetic storms, it is now known that CMEs are responsible for large storms (Gosling *et al.*, 1991; Kahler, 1992; Gosling, 1993). The geoeffectiveness of MCs arises from the fact that they can impose long periods of strong southward interplanetary magnetic field (IMF) on the Earth's magnetosphere (e.g., Russell *et al.*, 1974; Gonzalez and Tsurutani, 1987). The scientific importance of CMEs also lies in the fact that they may be an archetypal eruptive process; the physics of CMEs may shed new light on other puzzling eruptive phenomena such as flares.

The prevailing attempts to understand CMEs (and flares) are guided by the long-standing hypothesis that the energy of solar eruptions is stored in the corona and is built up by the quasi-static motion of the photospheric footpoints of the coronal field. We will refer to this hypothesis as the 'storage-release' paradigm. However, essentially all questions regarding the physical mechanism(s) of CMEs and flares have yet to be answered within this framework. In the meantime, the new ISTP observations of the Sun and the SW now demand that the correct theory must explain not only the observed CMEs but also the ejecta in the interplanetary medium.

This paper will briefly review CME research to date and describe a new theory that appears to correctly explain in a unified manner the dynamics of a class of observed CMEs and their evolution in the heliosphere. The basic hypothesis of the new theory differs from that of the storage-release paradigm in one fundamental area: the magnetic energy responsible for the eruption resides below the photosphere prior to the eruption and is dynamically 'injected' into the corona. The time scale is Alfvénic, neither quasi-static nor impulsive. In response, the flux rope expands at the Alfvénic speeds. The injected energy is entirely in the poloidal field and has been neglected in previous theories. If the apparent success of the new theory is validated, the theory points to a new paradigm for solar eruptions in general;

eruptions are the end products of dynamic Alfvénic relaxation of magnetic energy propagating outward from the solar dynamo. Potentially observable consequences of the theory will be discussed.

1. Physics Issues and Previous Works

1.1. MAGNETIC GEOMETRY

It is widely accepted that CMEs and other large-scale solar eruptions are driven by magnetic energy. Thus, one of the most important questions concerning CMEs is the structure of the underlying magnetic field because the Lorentz force ($\mathbf{J} \times \mathbf{B}$) and magnetic energy are determined by the distribution of the electric current and magnetic field. Unfortunately, there is as yet no *in situ* measurement of coronal magnetic field, and coronagraph data do not yield unique three-dimensional (3-D) interpretation of the observed two-dimensional (2-D) images. However, a number of hypotheses for CME magnetic structure have been advanced.

Early models of CMEs assumed that the bright rim (e.g., rim *A* in Figure 1) is a thin magnetic 'loop' or a 'flux rope' (Mouschovias and Poland, 1978; Anzer, 1978), but such loops appear to be more consistent with projections of structures with depths along the line of sight comparable to the widths (e.g., Howard *et al.*, 1982; Fisher and Munro, 1984; Webb, 1988). Considerable debate on the 3-D structure of CMEs persisted for over a decade (see, for example, a review by Hundhausen, 1999), but a key finding was that CMEs, when projected onto the plane of the sky, generally have a three-part morphology, consisting of a bright rim, followed by a relatively dark cavity, which often but not always contains a relatively bright core (Illing and Hundhausen, 1986). The CME shown in Figure 1 exhibits this prototypical morphology: the bright rim *A* encircles a cavity that, in this event, contains a core (arrow). The three-part morphology, however, did not clarify the magnetic field geometry in 3-D.

A simple geometry that is amenable to theoretical and numerical studies is that of magnetic arcades, illustrated in Figure 2. Topologically, this configuration is characterized by magnetic 'field lines' that are anchored in the photosphere. This configuration has been extensively used to study theoretical issues concerning the storage and release of magnetic energy in the corona, to be discussed below.

Recently, attention has shifted to erupting magnetic flux ropes as the underlying process in solar eruptions in general (Chen, 1989) and in CMEs and prominences in particular (Chen and Garren, 1993; Chen, 1990, 1996; Kumar and Rust, 1996; Wu *et al.*, 1999; Krall *et al.*, 2000). Figure 3(a) illustrates a flux rope. This is an attractive configuration because eruptive prominences, known to be associated with CMEs, often exhibit helical features that are presumed to indicate the underlying twisted field lines (e.g., Rompolt, 1975; Schmahl and Hildner, 1977; Vršnak *et al.*, 1991; Tandberg-Hanssen, 1995). Figure 3(b) shows an oblique view of a flux

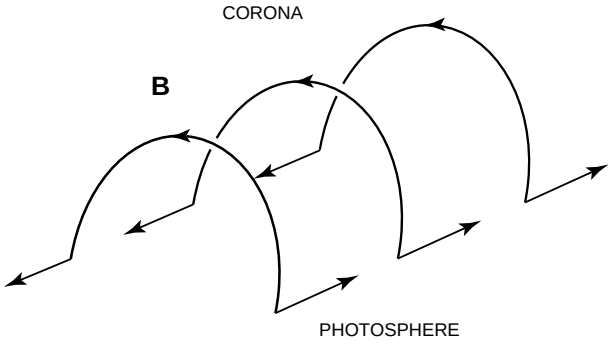

Figure 2. Schematic of a coronal arcade. Magnetic field lines are anchored in the photosphere, and their footpoints are oppositely sheared.

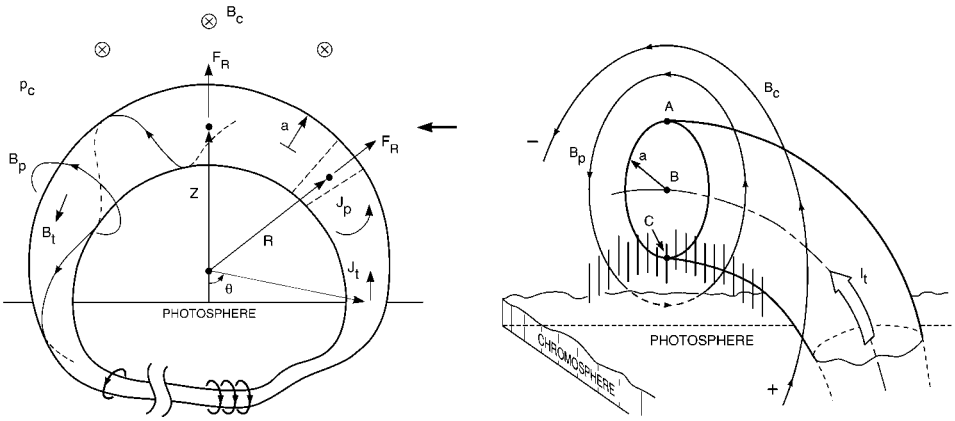

Figure 3. (a) (Left) Side view of a flux rope. The plane of the flux rope is in the plane of the paper. The subscripts '*t*' and '*p*' refer to toroidal and poloidal directions, respectively. The current channel has major radius R and minor radius a. 'Flux rope' refers to the entire structure, including the subphotospheric segment emanating from the dynamo ($\approx$). (b) (Right) Oblique view of a flux rope. The leading edge, the centroid, and the trailing edge of the current channel are indicated by A, B, and C, respectively. B_C is the overlying field outside the flux rope. The short vertical hashed lines indicate where the prominence may be located.

rope. The short vertical lines indicate the prominence. This is an 'inverse polarity' configuration (Kuperus and Raadu, 1974). The CME shown in Figure 1 has been interpreted as a flux rope viewed obliquely (Chen *et al.*, 2000). The equilibria of 3-D flux ropes have been analyzed using an integral MHD approach (Xue and Chen, 1983). Low and Hundhausen (1995) developed a model using a cylinderical flux rope with the prominence treated as a current sheet suspended against gravity by the Lorentz force.

Although it has been widely assumed that solar flux ropes are formed after potential (current-free) fields are twisted by photospheric motion, recent observational evidence indicates that flux ropes do emerge in twisted state (Tanaka, 1991;

Lites *et al.*, 1995; Leka *et al.*, 1996). Certain observed features of filaments are consistent with the interpretation that the magnetic field underlying a filament has the topology of a flux rope (Filippov, 1995; Low and Hundhausen, 1995; Aulanier *et al.*, 1999). We use the term 'magnetic topology' to connote 'magnetic connectivity' rather than geometry.

If the initial structure is a flux rope, a CME evolves into a MC without reconnection (Chen and Garren, 1993; Chen, 1996). Empirically, magnetic clouds appear to constitute $\frac{1}{3}$ (Gosling, 1990) or more (Webb *et al.*, 2000) of CMEs. In contrast, if the initial structure is an arcade, it must undergo large-scale reconnection to form a flux rope. Reconnecting current sheets in the corona have thicknesses of the order of the local ion gyroradius, and the dissipation region in reconnection is on the scale of the ion skin depth (Shay *et al.*, 1999). Both scales are much smaller than the relevant system sizes and the typical mean free paths. The role reconnection may play in large-scale eruptions in 3-D is not yet well understood.

1.2. Coronal energy storage and eruption

It is generally assumed that solar flares are powered by the release of magnetic energy stored in coronal magnetic fields (e.g., Gold and Hoyle, 1960; Svestka, 1976; Moore *et al.*, 1980; Sturrock, 1980). This assumption has been extended to CMEs. The basis for this concept is that (1) the eruptive phenomena exhibit release of energy and mass motions occurring much faster than any motion and time scales seen in the photosphere and (2) no significant systematic changes in the photospheric motions are apparent during eruptions. Mass motions associated with flares and CMEs occur at speeds of the order of $100-1000$ km s^{-1} compared to photospheric speeds of the order of 1 km s^{-1}. The first observation has led to the notion that there are two time scales, 'slow' in the photosphere and 'fast' in the corona, representing two intrinsically different types of physical processes, viz., quasi-static versus dynamic. Within the framework of magnetohydrodynamics (MHD) equations, the coronal field is assumed to evolve subject to the prescribed quasi-static motion of the photospheric footpoints (e.g., Gold and Hoyle, 1960; Sturrock, 1980; Aly, 1984; Mikić and Linker, 1994; Forbes and Priest, 1995; Parker, 1996; Antiochos *et al.*, 1999; Amari *et al.*, 1999). The photosphere is taken to be an infinitely conducting medium. A conceptually appealing corollary of the last assumption is that the solar interior can be decoupled from the coronal fields.

The conjecture is that a stressed coronal structure may rapidly release the stored magnetic energy if it reaches a critical point beyond which no equilibrium exists or some MHD instability sets in. A fundamental question in this paradigm, and indeed in modern theoretical solar physics, has been whether a coronal magnetic structure such as an arcade or a flux rope encounters a critical point under quasi-static evolution and whether, if such a critical point is exceeded, the stored magnetic energy can be impulsively released as flares and CMEs.

Specifically, bifurcations in 2-D equilibrium solutions have been studied (e.g., Low, 1977; Jockers, 1978; Birn *et al.*, 1978; Heyvaerts *et al.*, 1982; Zwingmann, 1987; Klimchuk and Sturrock, 1989; Finn and Chen, 1990; Mikić and Linker, 1994). It was found that quasi-static shearing of footpoints does not lead to bifurcated solutions in 2-D arcades (Zwingmann, 1987; Klimchuk and Sturrock, 1989; Finn and Chen, 1990) and in 3-D flux ropes (Chen, 1990). Increasing the internal energy (entropy) of an arcade also does not yield bifurcations (Finn and Chen, 1990).

It has been suggested that a magnetic structure may develop MHD instabilities such as the kink instability (e.g., Hood and Priest, 1979; Rust, 1994; Amari *et al.*, 1996; Lionello *et al.*, 1998). In these works, the flux rope is either a straight cylinder (e.g., Hood and Priest, 1979; Lionello *et al.*, 1999) or confined by numerical boundaries (Amari *et al.*, 1996). In contrast, an unconfined 3-D flux rope is stable to the kink mode (Chen, 1997). The reason is that a 3-D flux rope with no artificial confining influences can expand, reducing the pitch of the magntic field. In straight cylinders and confined 3-D flux ropes, the ability of the flux rope to expand is artificially inhibited.

The original idea of Gold and Hoyle (1960) is that neighboring flux ropes with sheared magnetic field interact with each other, annihilating the magnetic field due to magnetic reconnection and releasing the stored magnetic energy. Similarly, the interaction of sheared (and expanding) arcades with different forms of ambient magnetic field has been studied using MHD simulations (Mikić *et al.*, 1988; Biskamp and Welter, 1989; Finn *et al.*, 1992; Antiochos *et al.*, 1999). These studies show that an expanding arcade confined by ambient magnetic field or numerical boundaries can develop instabilities, resulting in reconnection between the arcade field and the surrounding coronal fields. The character of the instabilities, however, can be sensitive to the boundary conditions (Biskamp and Welter, 1989; Finn *et al.*, 1992). A related scenario is to invoke reconnection between a newly emerged magnetic structure and the preexisting coronal field (Heyvaerts *et al.*, 1977).

Another class of flare models is based on the idea that the photospheric flows across the footpoints of coronal field act as a dynamo and produce the sudden release of magnetic energy (Sen and White, 1972; Heyvaerts, 1974; Kan *et al.*, 1983; Akasofu, 1984; Hénoux and Somov, 1987). However, it has been pointed out (Melrose and McClymont, 1987; Melrose and Khan, 1989; Fisher and McClymont, 1989) that such models require too much electrical resistance in the photosphere, large unbalanced stresses on the neutral gas, and photospheric flows much faster than observed flow speeds.

Using a 2-D arcade geometry, Barnes and Sturrock (1972) argued that under quasi-static changes in the photospheric conditions, a force-free closed magnetic field structure builds up magnetic energy greater than that of the ‘open’ field configuration with the same photospheric boundary conditions. However, Aly (1984) argued that the upper limit for the magnetic energy of a closed force-free magnetic structure is that of the open field with the same normal component of the photo-

spheric magnetic field. This argument was later supported by Sturrock (1991). As a result, the question of energy storage has attracted renewed interest (e.g., Wolfson and Low, 1992; Mikić and Linker, 1994; Amari *et al.*, 1996). Wolfson and Saran (1998) showed that inclusion of gravity and an overlying streamer structure allows an arcade to store more magnetic energy. Recently, Antiochos *et al.* (1999) numerically showed that a 2-D force-free arcade can store magnetic energy in excess of the Aly energy limit if there is an overlying coronal field.

Using a simple but fully 3-D flux rope, Xue and Chen (1983) showed on the basis of force balance that the coronal pressure is insufficient to support magnetic energy in an isolated flux rope to power large solar flares. Fisher and McClymont (1989) also pointed out the difficulty of storing sufficient magnetic energy in the corona for large flares.

Thus, the fundamental issues of the storage-release paradigm, the dominant framework for models of solar eruptions for over four decades, have remained unanswered: (1) it is not yet established whether or how sufficient energy can be stored in the corona in 3-D to power eruptions; (2) it is not understood whether a realistic solar magnetic structure undergoing quasi-static motion of the footpoints possesses a critical point beyond which no equilibrium or stability exists; (3) no specific footpoint motion that can be directly related to observed eruptions has been documented; (4) there is as yet no model based on the storage-release paradigm that can correctly describe the observed dynamics of both CMEs and their heliospheric consequences (e.g., MCs).

2. A New Theory of CMEs

We now describe a theoretical model that adopts an entirely different hypothesis and that has produced quantitative results in essential agreement with both solar and SW observations.

2.1. TOROIDAL SELF FORCES

One of the most basic questions is what causes a massive structure of 10^{14-16} g to erupt. Here, we will summarize the basic MHD forces that act on a 3-D flux rope. The details have been discussed elsewhere (Chen, 1989; Garren and Chen, 1994).

A flux rope consists of a current channel ($\mathbf{J} \neq 0, r \leq a$) and the magnetic field $\mathbf{B}$ given by $\mathbf{J} = (c/4\pi)\nabla \times \mathbf{B}$. We will refer to this field as the 'private' field of the flux rope and distinguish it from the 'community' field arising from currents elsewhere. The coronal part of the current channel has major radius R and minor radius a, as illustrated in Figure 3(a). Inside the current channel ($r \leq a, \mathbf{J} \neq 0$), the current density has a toroidal (locally axial), $J_t(r)$, and a poloidal (locally azimuthal), $J_p(r)$, component, producing poloidal and toroidal magnetic field components, B_p and B_t, respectively. Here, r is the minor radial coordinate measured from the

minor axis. Inside the current loop, B_p and B_t are generally both nonzero, with helical or 'twisted' field lines. These field lines thread the photosphere. Outside the current channel ($r > a$, $\mathbf{J} = 0$), the magnetic field is purely poloidal irrespective of the form of $J_t(r)$, $r \leq a$. Topologically, poloidal field lines have no photospheric footpoints. One private poloidal field line is depicted (B_p). The poloidal field decreases rapidly outside the current channel and is assumed to vanish at infinity. On the minor axis, the magnetic field is purely toroidal. There is no one value of pitch angle for the field-line twist. The system is embedded in an ambient coronal density n_a and an overlying coronal magnetic field (B_c). The footpoints of the flux rope are assumed to be stationary because of the large photospheric mass density.

The current loop is assumed to be part of a larger current system extending below the photosphere and ultimately connected to the solar dynamo (indicated by $\approx$ in Figure 3(a)). It is important that the subphotospheric current/field connection to the source of magnetic energy exist, but no particular structure needs to be specified. The theory does not explicitly treat the dynamo or the transport of the magnetic energy along the flux rope below the photosphsere. However, it will be shown (section 4.1) that the basic nature of the transport process is Alfvénic relaxation.

Given a current loop, the poloidal flux enclosed by the loop and the photosphere can be written as $\Phi_p = cLI_t$, where L is the self inductance of the current loop above the photosphere, and I_t is the net toroidal current. The total poloidal flux of the loop above the photosphere is then

$$\Phi_p(t) = cL(t)I_t(t), \tag{1}$$

and the total poloidal magnetic energy above the photosphere is

$$U_p \equiv \tfrac{1}{2} LI_t^2. \tag{2}$$

An approximate form of L has been given elsewhere (Chen and Garren, 1993; Krall *et al.*, 2000) and is not repeated here. We only mention that L is a measure of the geometrical size of the current loop with $L \propto R$. Thus, L changes with time as the flux rope expands.

The toroidal flux is assumed to be conserved and is given everywhere along the flux rope (including the subsurface part) by

$$\Phi_t = \pi \overline{B}_t a^2 = \text{constant}, \tag{3}$$

where, $\overline{B}_t$ is the toroidal field averaged over the minor radius. The three dimensionality of the flux rope is embodied in the finite values of R, Φ_p, and U_p, all of which would be infinite in 2-D. There is no 2-D counterpart of the physics discussed here.

The MHD force acting on a plasma element is

$$\mathbf{f} = (1/c)\,\mathbf{J} \times \mathbf{B} - \nabla p + \varrho \nabla \varphi, \tag{4}$$

where ϱ is the mass density, and φ is the gravitational potential. The loop above the photosphere may be thought of as a section of a torus of major radius R and minor radius a. The integrated force acting in the major radial direction on a section of unit length is

$$F_R = \frac{I_t{}^2}{c^2 R}\left[\ln\left(\frac{8R}{a}\right) + \frac{1}{2}\beta_p - \frac{1}{2}\frac{\overline{B}_t^2}{B_{pa}^2} + \right. \\ \left. + 2\left(\frac{R}{a}\right)\frac{B_c}{B_{pa}} - 1 + \frac{\xi_i}{2}\right] + F_g + F_d, \tag{5}$$

where $\beta_p \equiv 8\pi(\overline{p} - p_a)/B_{pa}^2$, $\overline{p}$ is the average pressure inside the loop, p_a is the ambient pressure, $\overline{B_t}$ is the average toroidal field inside the loop, $B_{pa} \equiv B_p(r = a) = 2I_t/ca$, $\xi_i \equiv 2\int r B_p^2(r)\,\mathrm{d}r/(a^2 B_{pa}^2)$ is the internal inductance, and I_t is the total toroidal current $I_t \equiv 2\pi \int J_t(r) r\,\mathrm{d}r$. The actual form of $J_t(r)$ enters the analysis only through ξ_i and does not explicitly affect the other terms. The term F_g is the gravitational force per unit length. The momentum coupling between the flux rope and the ambient gas is modeled by the drag term F_d. The above expression has error terms of order (a/R) but has been found to be a good approximation for arbitrary $a/R \ll 1$ (Garren and Chen, 1994).

The apex motion is governed by

$$M\frac{\mathrm{d}^2 Z}{\mathrm{d}t^2} = F_R = \left(\frac{\Phi_p^2}{c^4 L^2 R}\right) f_R + F_g + F_d, \tag{6}$$

where f_R is simply the quantities in the square brackets in (5). The factor $(I_t^2/c^2 R)$ in (5) has been rewritten in terms of Φ_p and L using Equation (1). In (6), $M \equiv \pi a^2 \overline{n}_T m_i$ is the total mass per unit length of the loop, and Z is the height of the center of mass of the apex (point B in Figure 3(b)). The expansion of the rest of the loop is determined by assuming that the major radius $R(t)$ is uniform along the flux rope. The minor radius $a(t)$ of the apex evolves in time according to

$$M\frac{\mathrm{d}^2 a}{\mathrm{d}t^2} = \frac{I_t^2}{c^2 a} f_a, \tag{7}$$

where $f_a(t) \equiv (\overline{B}_t^2/B_{pa}^2 - 1 + \beta_p)$.

In the initial equilibrium, the forces are balanced everywhere, so that $F_R = 0$ and $f_a = 0$. If a packet of energy associated with the private poloidal flux of the flux rope propagates from the dynamo and rises into the corona, Φ_p in Equation (6) increases and the flux rope deviates from equilibrium. We refer to this process as 'injection' of poloidal flux. Physically, the profile of the injection rate, $\mathrm{d}\Phi_p/\mathrm{d}t$, is determined by the dynamo action and the propagation characteristics in the convection zone, but in the model, $\mathrm{d}\Phi_p/\mathrm{d}t$ is prescribed. Equations (6) and (7), along with several ancillary conditions including Equations (1) and (3), are the basic equations

of the model. See Chen (1996) for a complete description of the model system, including a model solar wind. The initial-value solutions describe the eruption of CMEs and the subsequent dynamics through the interplanetary medium. Note that Aly's (1984) energy limit is irrelevant if there is flux injection.

The term 'injection' is used to emphasize that the poloidal flux is added to the existing coronal structure and to distinguish this process from those where 'emerging flux' triggers the release of the stored energy (e.g., by reconnection). In the former case, it is the private flux that emerges, while in the latter case, community flux emerges.

2.2. Comparison of theory and CME observations

Equations (6) and (7) have been tested against several observed CMEs using the recent data obtained by LASCO and MK3 and by the Extreme Ultraviolet Imaging Telescope (EIT) on board SOHO.

Figure 4 shows the LASCO C2 coronagraph image taken at 16:36 UT, 1997 April 13. The white semi-circle on the left is the western half of the Sun and the semi-circular region outside the Sun is the occulting disk of radius $\simeq 2\ R_\odot$. The image clearly shows a bright rim marked A encircling a relatively dark cavity containing bright prominence material. The structure exhibits the prototypical 3-part CME morphology (Illing and Hundhausen, 1986). Within the nearly circular rim A, the leading edge (a), the top (b) and bottom (c) edges, and the trailing edge (e) are marked. The centroid of rim A is indicated by d. In addition, the bright features marked E_1 and E_2 remain connected to the outer edge of the occulting disk, and are interpreted as evidence of magnetic connection between the CME and the Sun.

The above features have been identified as the basic morphological features of a 3-D flux rope projected onto the 2-D plane of the sky by Chen *et al.* (1997), who interpreted the observed CME-cavity structure as the projection of a 3-D flux rope lying in the ecliptic plane with the legs connected to the Sun and viewed end-on. This corresponds to a view along the arrow on the right in Figure 3(a). The motion of the observed features can be accurately explained by the erupting flux rope model of Chen (1996). Wood *et al.* (1999) examined two CME events that exhibited nearly identical flux rope features to those of the April 13 CME. These events were well observed by EIT, C1, C2, and C3 instruments. One CME was fast ($\sim$900 km s^{-1}), and the other was relatively slow ($\sim$300 km s^{-1}). They found that the theory was able to properly model the early times for both events. Several CMEs exhibiting the flux rope morphology have been examined in detail (Dere *et al.*, 1999). More recently, the fast CME of 1997 September 9 (Figure 1) was shown to be fully consistent with a 3-D flux rope viewed obliquely (Chen *et al.*, 2000), a nearly orthogonal view to that of the April 13 CME. There appears to be a class of CMEs that can be quantitatively and morphologically understood as erupting flux ropes.

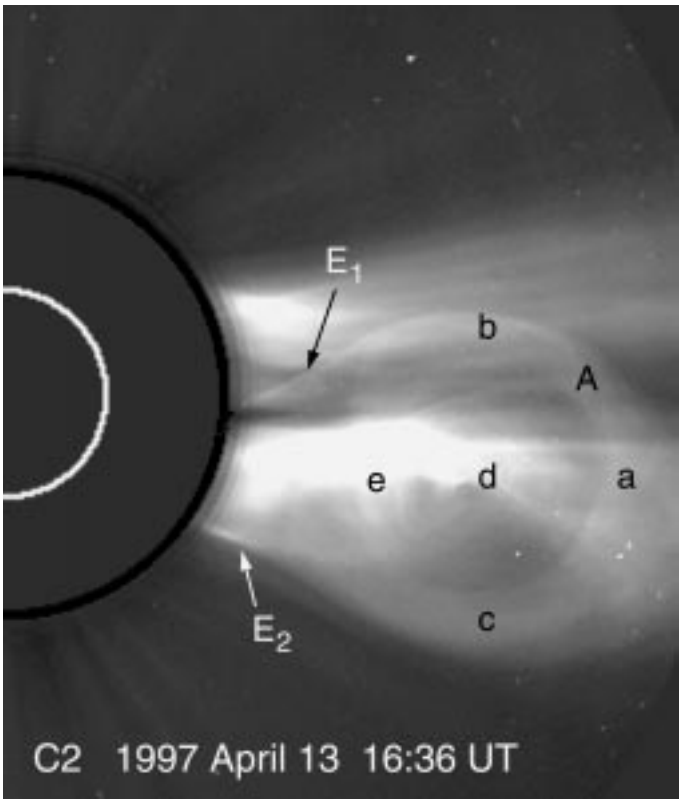

Figure 4. LASCO CME of 1997 April 13, showing features interpreted as the projection of a flux rope. From Chen *et al.* (1997).

Figure 5 shows the measured motion of several features of the CME of 1997 September 9. Figure 5(a) shows the positions of the leading edge (a in Figure 1) represented by squares and the centroid (the midpoint between b and c in Figure 1) represented by circles. In these panels, the solid symbols show the MK3 and C3 data points and the open symbols the C2 data. The solid and dashed curves show the theoretical results corresponding to *a* and the centroid, respectively. Figure 5 shows good agreement between the theoretical results and the observed CME motion throughout the MK3 and LASCO fields of view.

It is noteworthy that the solution is able to match nontrivial acceleration and speed profiles (Figure 5(c)) as well as the aspect ratio $\Lambda \equiv Z_s/D$ (Figure 5(b)), where $Z_s = Z + R_\odot$ is the height from Sun center and D is the distance between b and c. In particular, the larger values of Λ in early times (MK3 data) result from the flux injection ($\mathrm{d}\Phi_p/\mathrm{d}t$). The good agreement evident in Figure 5(b) means that the expansion of the CME in the direction transverse to the radial motion away from the Sun is replicated by the model equations. That is, the motions in the two orthogonal directions are correctly reproduced, further supporting the hypothesis

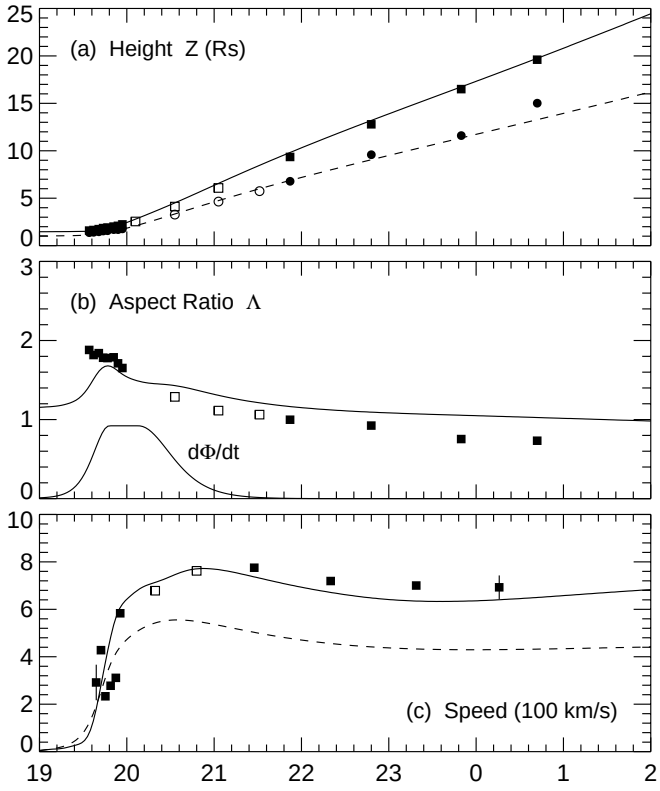

Figure 5. Comparison of theory and the CME of 1997 September 9. (a) The leading edge (a in Figure 1, solid curve) and the centroid (the midpoint of b and c, dashed curve) positions of the bright rim *A* are shown. The solid symbols are MK3 and C3 data. The open symbols are C2 data. (b) The aspect ratio and the poloidal flux injection profile, $d\Phi_p/dt\ (t)$. (c) The measured speeds of the leading edge a. The theretical results are shown for the leading edge a (solid curve) and the centroid (dashed curve). From Chen *et al.* (2000).

that the CME was indeed a magnetic flux rope, driven by poloidal flux injection. The near-constantcy of Λ in C2 and C3 was also found in other flux-rope CMEs studied to date..

The magnetic connectivity of CMEs to the Sun has been an important issue. Most previous models of CMEs call for disconnection of large-scale 'plasmoids' from the Sun, and observational evidence of such disconnection has been sought (e.g., Illing and Hundhausen, 1983; McComas *et al.*, 1991; Webb and Cliver, 1995). The persistence of E_1 and E_2 in the 1997 April 13 event suggests magnetic connection throughout the eruption process. In the 1997 September 9 CME, evidence of structural connection is stronger because the cavity under the rim *A* in Figure 1 is seen to be smoothly connected to a low-density cavity in MK3 and then to a 'dim' region in EIT images (Chen *et al.*, 2000). No evidence of disconnection was observed. Certain particle signatures at 1 AU (Larson *et al.*, 1997) and theoretical

argument (Chen and Garren, 1993) also indicate that MCs remain connected to the Sun.

2.3. INTERPLANETARY CONSEQUENCES

The heliospheric consequences of CMEs have been a long standing question. Although the evolution of CMEs beyond the fields of view of coronagraphs has not been observed, there has been clear statistical association between CMEs and MCs (e.g., Wilson and Hildner, 1984; Zhang and Burlaga, 1987; Gosling, 1990). Largely thanks to the ISTP program, the CME-MC connection has become stronger based on specific individual events (Burlaga *et al.*, 1998; Webb *et al.*, 2000). The latter work showed that during one period of time, all six Earth-directed halo CMEs were followed by MCs at 1 AU. Direct confirmation of the dynamical connection between CMEs and MCs, however, must await future observations. Nevertheless, the available data do provide a stringent constraint on any proposed CME models: a viable model must produce both correct CME eruptions and SW structures such as magnetic clouds that are observed to be associated with CMEs.

Theoretically, it has been shown using generic solar flux ropes that the initial-value solution that fits a CME evolves into a flux rope closely resembling observed MCs out to about 5 AU (Chen and Garren, 1993; Chen, 1996). The solutions that fit the April 13 and September 9 CMEs as well as several other observed CMEs also lead to interplanetary flux ropes consistent with observed MCs (Chen *et al.*, 1997, 2000; Krall *et al.*, 2000). These results are supported by numerical simulations of an expanding flux rope (Wu *et al.*, 1999).

Krall *et al.* (2000) further studied the consequences of several initiation and driving mechanisms including the injection of poloidal flux and slow twist of the photospheric footpoints (storage-release). They found that some scenarios are able to reproduce CME dynamics to varying degrees of success but that only the injection of poloidal flux can reproduce observed CMEs and observed MCs. Thus, based on quantitative comparisons between the model results and solar and SW observations, the toroidal flux rope model with injection of poloidal flux appears to correctly capture the essential physics of the CME-MC phenomenon. Note that the model results reproduce the specific properties of magnetic clouds in terms of physical quantities such as the size, magnetic field vector, and internal temperature (Burlaga *et al.*, 1981; Burlaga, 1988; Lepping *et al.*, 1990).

There is as yet no model based on the storage-release paradigm that can quantitatively describe observed CME dynamics, much less the subsequent propagation. The key concept underlying the new theory is the dynamical connection between the subsurface energy source and coronal eruptions via the transport of poloidal magnetic energy, first suggested by Chen (1989, 1990).

3. A New Paradigm: Alfvénic Relaxations as Solar Eruptions

3.1. POLOIDAL FLUX TRANSPORT AND PLASMA MOTION

As one output of the model, it was found that the poloidal flux should be injected over several hours to obtain the best fit to the observed CMEs (Chen *et al.*, 1997, 2000; Wood *et al.*, 1999; Krall *et al.*, 2000). This time is neither impulsive nor quasi-static. An important question is how the photosphere responds to the passage of a substantial amount of magnetic energy. We will show below that this process is Alfvénic.

Returning to Figure 3(a), let the entire flux rope system be in equilibrium. This means that the forces are balanced everywhere along the flux rope. We do not explicitly consider the dynamo, presumed to be located deep in the convection zone, except to state that it produces and maintains the toroidal current and poloidal flux. The toroidal flux is not altered by the dynamo and is conserved. Now suppose that the dynamo action increases, i.e., the toroidal current, or equivalently, the poloidal flux is increased in the dynamo region. This means that the system deviates from the initial equilibrium near the source. This is illustrated in Figure 3(a), where the poloidal field lines ('rings') near the dynamo ($\approx$) represent the flux in excess of the equilibrium magnetic field. The system is now out of equilibrium in this region and must redistribute the excess energy to reach a new equilibrium.

The process of relaxing to a new equilibrium entails motion of the flux rope and the ambient plasmas. The magnetized fluid motion is governed by the force (4). Consider the Lorentz and the pressure forces

$$\varrho \frac{\mathrm{d}\mathbf{v}}{\mathrm{d}t} = \frac{1}{c}\mathbf{J} \times \mathbf{B} - \nabla p. \tag{8}$$

Using the identify

$$\mathbf{J} \times \mathbf{B} = \frac{c}{4\pi}\left(\mathbf{B} \cdot \nabla \mathbf{B} - \nabla \frac{B^2}{2}\right),$$

we obtain the scaling

$$\varrho \frac{\mathrm{d}\mathbf{v}}{\mathrm{d}t} \sim \frac{1}{4\pi}\frac{B^2}{d} + \frac{p}{d}, \tag{9}$$

where d is the gradient scale length. Thus, in normalized form we have

$$\frac{\mathrm{d}\tilde{v}}{\mathrm{d}\tilde{t}} \sim 1, \tag{10}$$

where the normalized quantities are $\tilde{v} \equiv v/V_M$ and $\tilde{t} \equiv t/\tau_M$. Here, $V_M \equiv (V_\mathrm{A}^2 + C_s^2)^{1/2}$, where $V_\mathrm{A} = B/(4\pi\varrho)^{1/2}$ and $C_s = (\gamma p/\varrho)^{1/2}$ are the local Alfvén and sound speeds, respectively. The time scale is

$$\tau_M \equiv \frac{\mathrm{d}}{V_M}.$$

Note that $V_A/C_s \propto \beta^{-1/2}$, so that for $\beta \ll 1$ ($\beta \gg 1$), $V_A \gg C_s$ ($V_A \ll C_s$). The gravity term introduces buoyancy and convection and is not included here for the discussion of magnetic energy.

Thus, if a system whose motion is governed by Equation (8) is forced out of equilibrium, it tends to relax to a new equilibrium with

$$\frac{v}{V_M} \lesssim 1. \tag{11}$$

Equations (6) and (7) both exhibit this property, with $f_R = 0$ and $f_a = 0$ in equilibrium and $f_R \lesssim 1$ and $f_a \lesssim 1$ when disturbed out of equilibrium. The characteristic speed is the Alfvén (magnetosonic) speed parallel (perpendicular) to the magnetic field. We use the term 'Alfvén' or 'Alfvénic' to refer to motion given by (11). Note that V_M is based on the field, pressure, and density of the plasma structure under consideration.

It should be pointed out that Equation (10) is strictly valid only locally because V_M is not constant. Nevertheless, it shows that given the basic equation of motion (8), the response of the flux rope and the ambient plasmas to increased magnetic energy is everywhere an Alfvénic relaxation process, be it the convection zone, the corona, or the heliosphere. The poloidal energy generated by the dynamo is redistributed along the flux rope by this process.

Let us now consider the implications of the above result for the photosphere and the corona, because these regions are accessible to direct observations. Figure 6 schematically depicts one leg of a flux rope (see Figure 3(a)) extending from below the photosphere into the corona. The footpoint structure consists of the current channel (carrying toroidal current I_t) and the private poloidal field. Several poloidal field lines are depicted by 'rings' with one such field line indicated by B_p. Also shown in the figure are two field lines, marked by B_c, indicating the ambient community field arising from currents external to the flux rope current. The private and community magnetic fields do not mix in highly conducting systems and must be distinguished. This means that where the two flux systems meet, current sheets are formed to accomodate the local gradients and shear in the magnetic field and pressure. If the footpoint consists of filamented current distributions. It is taken to be the net toroidal current of the flux rope.

The Alfvén speed in the photosphere can be estimated by

$$V_{ph} \simeq 2 \left(\frac{B}{100\ \mathrm{G}} \right) \left(\frac{10^{16}\ \mathrm{cm}^{-3}}{n} \right)^{1/2}\ \mathrm{km\ s}^{-1}. \tag{12}$$

Magnetic fields in the photosphere are typically concentrated in thin flux 'tubes' with 1–2 kG fields. Outside such flux tubes, the field may be an order of magnitude weaker. Thus, $V_{ph} \sim 20$ km s^{-1} if $B = 1$ kG and $V_{ph} \sim 2$ km s^{-1} if $B = 100$ G. The sound speed at 5000 K is $C_s \sim 11$ km s^{-1} ($\gamma = \frac{5}{3}$). The speed of mass motion due to the magnetic relaxation is some fraction of $V_M \sim 1$–10 km s^{-1}. The characteristic speed deeper in the convection zone may be slower.

In the corona, $n \sim 10^8$ cm^{-3} and $B \sim 10$ G in a flux rope, yielding

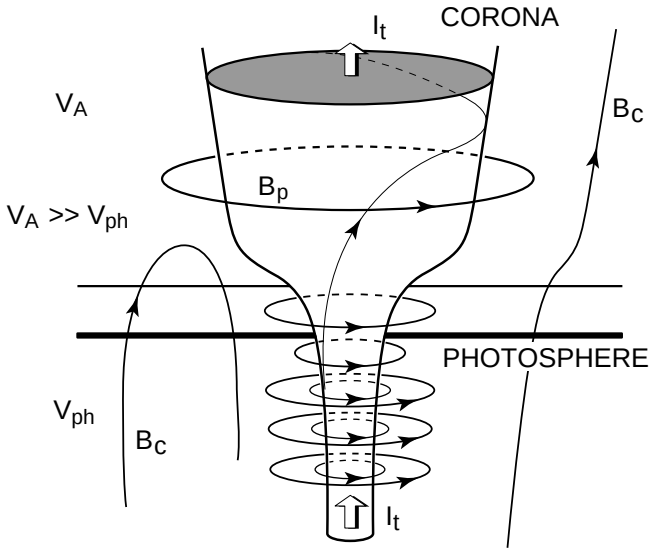

Figure 6. Schematic of a flux rope leg through the photosphere. The current channel carrying I_t, the top of which is shaded, and the private poloidal field (B_p) are shown. Two community field lines are shown (B_c). The magnetosonic speeds in the corona (V_A) and the subsurface ($V_p h$) with the ordering $V_M \gg V_{ph}$ are indicated.

$$V_A \simeq 2 \times 10^3 \left(\frac{B}{10\ \mathrm{G}}\right)\left(\frac{10^8\ \mathrm{cm}^{-3}}{n}\right)^{1/2}\ \mathrm{km\ s}^{-1}. \tag{13}$$

For coronal flux ropes, $\beta \ll 1$, so that $V_M \simeq V_A$; $V_M \simeq V_A \sim 2000$ km s^{-1}. Outside the flux rope, the B field is typically a few times weaker than the axial field (Chen, 1996), so that V_A is slower. The characteristic speed in the corona is much faster than that in the subphotosphere.

The key justification for the traditional quasi-static storage paradigm is the observation that during 'eruptive' events such as flares and CMEs, the photosphere exhibits no unusual motions (e.g., Rust, 1972). This has led to the notion that there are two time scales, one quasi-static and the other impulsive, and that the physically valid boundary conditions must be quasi-static shearing of the footpoints. This is particularly attractive from the theoretical point of view because it allows one to argue that the solar interior is dynamically decoupled from the corona and that the energy for eruption is stored in the corona.

The above analysis, Equations (8)–(11), shows that this assertion is incorrect: the photospheric motion is Alfvénic ($\mathrm{d}\tilde{v}/\mathrm{d}\tilde{t} \sim 1$), not quasi-static ($\mathrm{d}\tilde{v}/\mathrm{d}\tilde{t} \sim 0$). That is, Equation (10), which is applicable to both the photosphere and the corona, does not distinguish between the two regions. The perception of 'fast' coronal speeds and 'slow' photospheric speeds arises because two mediums with disparate characteristic speed are observed. Objectively, the same physics, $\mathrm{d}\tilde{v}/\mathrm{d}\tilde{t} \sim 1$, gov-

erns both regions. Photospheric motions are no slower than coronal motions relative to the characteristic speeds of the respective mediums.

Observationally, the photospheric plasmas already move at their local characteristic speeds in response to energy percolating up, and poloidal flux transport through the region can produce no faster motion than the typical motions. There may, however, be uniquely characteristic patterns of motions caused by poloidal flux transport superimposed on the more random motions that are typically seen. Such patterns may be observable if the more random motion of comparable speeds can be subtracted out. There is as yet no theoretical calculation of photospheric signatures caused by the poloidal flux injection. However, a 1-D MHD simulation study has been carried out (Huba and Chen, 1996). The results indicate that the photospheric speeds of tens of meters per second arise in response to a magnetic 'piston'. The speeds can reach a few hundred kilometers per second at the base of the corona. These results clearly show that the plasma motion is Alfvénic, satisfying $v/V_M \lesssim 1$ throughout these regions.

3.2. THE DYNAMICAL TIME SCALE

We now consider the time scale of eruption in relation to the flux injection profile. For the fast CME described in Figure 5, the solution shows that the duration of poloidal flux injection is approximately 2.5 hours. The specific profile of $(\mathrm{d}\Phi_p/\mathrm{d}t)$ has a ramp-up time scale of 15 min, reaching the peak value in about 50 min. For the slower 1997 April 13 CME, the durations of flux injection for good fits are 4–6 hours (Chen *et al.*, 1997). For the events modeled by Krall *et al.* (2000), poloidal flux is also injected over several hours. Thus, the model predicts that the observed CMEs correspond to poloidal flux injection on time scales of several hours.

An important question is whether the observed height-time profiles are artificially determined by the profile of $\mathrm{d}\Phi_p/\mathrm{d}t$. To test this point, the initial structure used to model the 1997 September 9 CME has been driven with a $\mathrm{d}\Phi_p/\mathrm{d}t$ profile with a ramp-up time scale of 5 min. This is roughly $\frac{1}{3}$ of the time scale used for the solution shown in Figure 5, providing a much more impulsive injection profile. Figure 7 shows the results. Comparing Figure 7(b) with Figure 5(b), we see that the flux injection rate increases much more steeply. However, Figure 7(a) shows that the leading edge and the centroid positions can be modeled to the same degree of accuracy as the profile shown in Figure 5(a). The injection profile used for Figure 7 corresponds to 3.3×10^{32} erg of poloidal energy, comparable to 3.5×10^{32} for the profile in Figure 5.

Although the two profiles of $\mathrm{d}\Phi_p/\mathrm{d}t$ give similar CME behaviors, there are differences. The most notable is the presence of oscillations in the calculated leading edge trajectory in the early times (solid curve, Figure 7(c)). This arises from minor radial oscillations superimposed on the centroid motion. The centroid speed profile (dashed curve, Figure 7(c)) is nearly identical to that in Figure 5(c). The minor radial oscillation occurs in this example because the rapid injection of the poloidal

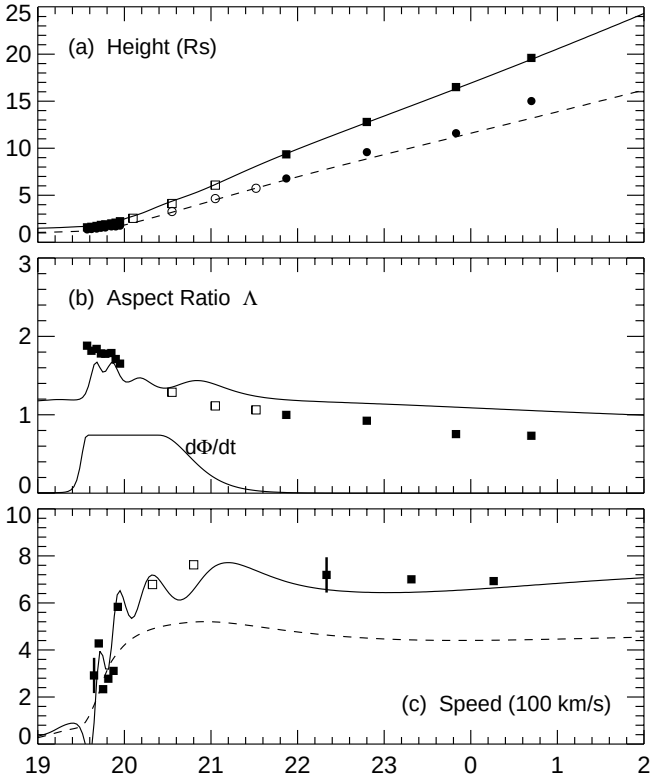

Figure 7. Modeling of the September 9 CME (Figure 1). The $d\Phi_p/dt\ (t)$ has a much steeper ramp-up profile compared to that in Figure 5(b). (a) Leading edge (a) and centroid positions (same data points as in Figure 5(a)). (b) Aspect ratio Λ and the prescribed $d\Phi_p/dt\ (t)$. (c) Calculated speeds of the leading edge (solid) and centroid (dashed). Data points show the observed leading-edge speed (projected).

flux increases pinch force and causes the transient ringing. It is interesting to note that the MK3 data points do indicate that at ∼19:50 UT the speed decreased from ∼420 km s^{-1} to ∼220 km s^{-1}. This was also noted by Chen *et al.* (2000), but they did not model it because of the relatively large errors in calculating the velocity. (The MK3 data, when viewed in the movie format, show slight 'hesitation' by the leading edge.) The relative insensitivity to the imposed profile of $d\Phi_p/dt$ was also noted for the 1997 April 13 event (Chen *et al.*, 1997).

The fact that the overall acceleration of the flux rope as indicated by the centroid motion is virtually unchanged by the more impulsive $d\Phi_p/dt$ profile is important because it shows that the acceleration time scale is not sensitive to the imposed injection profile. The time scale of major radial expansion in the initial linear regime, has been analytically calculated (Chen, 1989, equation (21)) and scales as

$$T \sim \frac{2M^{1/2}}{B_{pa}} \frac{R}{a} \propto \frac{R}{V_{Ap}}, \tag{14}$$

where V_{Ap} is the Alfvén speed based on B_{pa}. The actual time is this quantity multiplied by a factor of order unity. This means that to lowest order the acceleration time scale is determined by the inertia and the magnetic field of the flux rope and is proportional to the Alfvén transit time across the major radius. Figure 7(c) shows both the linear and nonlinear behaviors. Note that if the injection time scale is much longer than T above, then the flux rope rises quasi-statically (Chen, 1990).

It is easy to show from Equation (7) that the period of minor radial oscillations is of the order of $\tau_a \equiv a/V_{Ap}$. For the initial flux rope of Figure 5, $B_{pa} = 2.7$ G, $\varrho = 3.2 \times 10^{-16}$ g, and $a_0 = 1.56 \times 10^5$ km, and we have $\tau_a \simeq 8$ min. Figure 7(c) shows that the first few oscillations indeed have periods of approximately 10 min.

The time scale of poloidal flux injection, several hours, is an output of the model, not an imposed quantity. Although the definitive test of this process would require high-resolution and high-cadence vector magnetograph observation, we can ask a more generic question: does a significant amount of magnetic energy transit the photosphere in several hours? Observations of emerging flux regions (EFRs) shed light on this question. Although the tangential field is not specifically observed, EFRs represent the appearance of new magnetic structures and may serve as an indicator of the time scale on which significant magnetic energy is transported through the photosphere. For example, an EFR was observed to appear between two successive Hα images separated by about 5.5 hours (Brueckner *et al.*, 1988). Schrijver *et al.* (1999) presented detailed high-cadence TRACE data on an emerging flux event on 1998 June 8. The data show that at about 02:40 UT a loop system started to emerge near the northwest limb. The loop system was well-established by about 04:30 UT. The region continued to show appearance of new flux for more than a day. Individual loops seem to appear in tens of minutes. The data clearly show that a substantial amount of magnetic flux does emerge through the photosphere in several hours. The predicted time scale appears to be fully consistent with the appearance of magnetic fields through the photosphere.

3.3. POLOIDAL FIELD NEAR THE PHOTOSPHERE

An important aspect of the injection of poloidal flux is that the poloidal magnetic field maintains no topological connection to the photosphere. Thus, the storage-release paradigm that seeks to build up energy in the corona by shearing footpoints entirely neglects the poloidal flux. As is evident from Figure 6, the twisted field lines exist inside the current channel, but most of the poloidal energy is outside the current channel (this can be shown easily but is only stated here).

For the 1997 September 9 CME, the predicted footpoint magnetic field variation at the base of the corona is shown in Figure 8. Notice that B_p increases from the initial value by about 40%. Increased B_p lasts about 50 min. The more impulsive an eruption is, the greater the amount of increase is. Comparing Figure 8 with

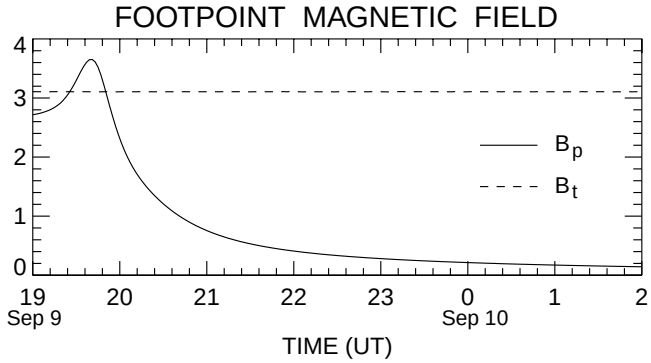

Figure 8. Poloidal and average toroidal components of a flux rope footpoint at the base of the corona. B_{pa} and $\overline{B}_t$ are plotted in gauss versus time. In the current channel ($r < a$) the field is nearly toroidal by 21:00 UT. The toroidal field on the axis is $\simeq 3\overline{B}_t$.

Figure 5, we see that B_p reaches its peak and begins to decrease when the major radial speed becomes significant. See Chen (1996) for a detailed discussion. The same physical process causes the aspect ratio Λ to peak at the same time. Subsequent to the initial period, B_p, which is tangential to the solar surface, decreases monotonically because of the rapidly increasing $L(t)$, and the magnetic field becomes essentially radial after the main acceleration phase even as the poloidal flux is injected (Figure 7(b)). Note that B_p shown in Figure 8 is the private flux of the flux rope. No contribution from the ambient medium is included. In general, the measured B_p need not vanish, and the fractional variation may be smaller than is suggested by Figure 8.

For the example discussed here, if the photospheric footpoint is such that the toroidal field on the axis ($3\overline{B}_t$) is 1 kG, the minor radius is smaller by a factor of 10, and the B_p profile in Figure 8, which is obtained for the base of the corona, should roughly scale up by a factor of 10. The peak in B_p, however, must be recomputed using the appropriate mass density.

The poloidal field B_p is tangential to the solar surface. The variation in B_p is subtle but potentially detectable by high-resoution vector magnetographs. To detect this effect, time cadences of a few minutes are necessary to resolve the characteristic variations shown in Figure 8. No systematic measurements of tangential fields with sufficient spatial and time resolution have been made to test the above prediction. Validation of this prediction must await future observtions. It is interesting to note, however, that changes in the tangential fields have been observed in association with large (X class) flares (Wang *et al.*, 1994; Cameron and Sammis, 1999). Such events are possibly more impulsive, thus exhibiting greater fractional vartiations due to the same physics.

4. Summary

The physical mechanisms of solar eruptions such as flares and CMEs have been a vexing question in solar physics. For over four decades, theories of eruptions have been guided by the storage-release paradigm. This concept is based on the unexamined assumption that the energy of eruptions is quasi-statically built up in the corona by the 'slow' motion of the photospheric footpoints of the coronal field. The stored magnetic energy is then released by some loss of equilibrium or instability. However, no specific motion of photospheric footpoints that is directly relatable to observed eruptions has been documented. To date, this paradigm has not produced a successful quantitative model of CMEs and other eruptions. The identification that the photospheric motions are quasi-static while the coronal motions are 'eruptive' is based on the subjective comparison of 'slow' photospheric and 'fast' coronal speeds. It is argued that this is an essential misidentification, arising from the fact that two distinct mediums with disparate characteristic speeds are observed. Normalized to the local Alfvén speed the plasma motions in both regions are described by the same physics, $\tilde{v} \lesssim 1$.

In contrast, the poloidal-flux injection hypothesis proposes that the CMEs and perhaps solar eruptions in general are driven by the injection of the *private* poloidal flux of existing flux ropes, which then relax at the coronal speeds. The coronal flux ropes are viewed as the 'tips' of much larger (and complicated) subphotospehric magnetic structures that are ultimately connected to the solar dynamo, thus having a direct conduit of energy from the source. A quantitative theory of CMEs based on this hypothesis has been developed. This theory describes CMEs as flux ropes expanding in response to the poloidal field 'injected' from below and yields MCs as the heliospheric consequence of CMEs. Detailed comparisons of the theoretical results with observed CMEs and MCs show good agreement. The theory provides the first unified description of the physics of CMEs and MCs, and its apparent success suggests a new paradigm for solar eruptions: the eruption and the outward expansion of coronal structures are merely an Alfvénic relaxation process in response to the magnetic energy reaching the corona from a deeper source. The motion of the flux system and the ambient plasma is everywhere governed by $\mathrm{d}\tilde{v}/\mathrm{d}\tilde{t} \sim 1$. Note that the storage-release paradigm, by virtue of the assumed infinite conductivity and infinite mass of the photosphere, precludes the transport of magnetic field through the photosphere from below on the time scale of eruptions. The photosphere, however, is merely an optical boundary, with no known ability to preclude magnetic energy transport from below, a region with much higher mass and energy densities.

Because the poloidal field has no topological footpoints in the photosphere, the poloidal energy is not accessible by the boundary conditions used to move footpoints. The photospheric motion in response to the poloidal flux injection occurs at $\tilde{v} \lesssim 1$. This is comparable to the ubiquitous motions caused by energy percolating up from below and may be difficult to observe. The injection of poloidal flux (Φ_p)

is predicted to result in characteristic changes in the poloidal field at the base of the corona down to the top of the photosphere. These changes are subtle but may be detectable by future vector magnetograph observations. Note that the profile ($d\Phi_p/dt$) and the amount ($\Delta\Phi_p$) of poloidal flux injection determine the acceleration profile (given the flux rope mass) and the magnitude of the magnetic field in the heliosphere, e.g., at 1 AU. Thus, the hypothesis of poloidal flux injection is potentially testable by observations of the tangential field in the photosphere as well as by *in situ* observations in the solar wind. The energy associated with the poloidal (i.e., tangential) field has been neglected from previous observational and theoretical considerations.

Finally, several major observational and theoretical issues for further studies are summarized. (1) The magnitude and the time variation of the poloidal magnetic fields at the footpoints of erupting magnetic flux ropes need to be observed with sufficient spatial and temporal resolution. (2) The pattern(s) of subtle photospheric plasma motions in response to the injection of poloidal flux need to be computed and tested against observations. (3) Ultimately, the possible profile of $d\Phi_p/dt$ must be computed from a first-principle theory of poloidal energy propagation along flux ropes in the convection zone. The structure of the subsurface part of a flux rope is unknown and requires further research. Tests (1) and (2), however, should be able to answer whether poloidal (tangential) flux is injected in relation to the observed eruption.

Acknowledgements

I wish to thank my colleagues, especially J. Krall and J. D. Huba, for stimulating discussions. This work was supported by the Office Naval Research. The SOHO/LASCO data used here are produced by a consortium of the Naval Research Laboratory (USA), Max-Planck-Institüt für Aeronomie (Germany), Laboratoire d'Astronomie (France), and the University of Birmingham (UK). SOHO is a project of international cooperation between ESA and NASA. The MK3 data are courtesy of the High Altitude Observatory/NCAR.

References

Akasofu, S.-I.: 1984, *Planetary Space Sci.* **32**, 1469.
Aly, J. J.: 1984, *Astrophys. J.* **283** 349.
Amari, T., Luciani, J. F., Aly, J. J. and Tagger, M.: 1996, *Astrophys. J.* **466**, L39.
Amari, T., Luciani, J. F., Mikić, Z. and Linker, J.: 2000, *Astrophys. J.* **529**, L49.
Antiochos, S. K., DeVore, C. R. and Klimchuk, J. A.: 1999, *Astrophys. J.* **510**, 485.
Anzer, U.: 1978, *Solar Phys.* **57**, 111.
Aulanier, G., Démoulin, P., Mein, N., van Driel-Gesztelyi, L., Mein, P. and Schmieder, B.: 1999, *Astron. Astrophys.* **342**, 867.

Barnes, C. W. and Sturrock, P. A.: 1972, *Astrophys. J.* **174**, 659.
Billings, E. E.: 1966, *A Guide to the Solar Corona*, Academic Press, New York, Chapter 6.
Birn, J., Goldstein, H. and Schindler, K.: 1978, *solar Phys.* **57**, 81.
Biskamp, D. and Welter, H.: 1989, *Solar Phys.* **120**, 49.
Brueckner, G. E., *et al.*: 1995, *Solar Phys.* **162**, 357.
Brueckner, G. E., *et al.*: 1998, *Geophys. Res. Lett.* **25**, 3019.
Burlaga, L. F.: 1988, *J. Geophys. Res.* **93**, 7217.
Burlaga, L. F., Sittler, E., Mariani, F. and Schwenn, R.: 1981, *J. Geophys. Res.* **86**, 6673.
Burlaga, L. F., *et al.*: 1998, *J. Geophys. Res.* **103**, 277.
Cameron, R. and Sammis, I.: 1999, *Astrophys. J.* **525**, L61.
Carrington, R. C.: 1860, *Monthly Notices Royal Astron. Soc.* **20**, 13.
Chen, J.: 1989, *Astrophys. J.* **338**, 453.
Chen, J.: 1990, in C. T. Russell, E. R. Priest, and L. C. Lee (eds), *Physics of Magnetic Flux Ropes*, *Geophys. Monogr. Ser.*, vol. 58, eds. AGU, Washington, D.C., p. 269.
Chen, J.: 1996, *J. Geophys. Res.* **101**, 27499.
Chen, J. and Garren, D. A.: 1993, *Geophys. Res. Lett.* **20**, 2319.
Chen, J., *et al.*: 1997, *Astrophys. J.* **490**, L191.
Chen, J., *et al.*: 2000, *Astrophys. J.* **533**, 481.
Dere, K. P., Brueckner, G. E., Howard, R. A. and Michels, D. J.: 1999, *Astrophys. J.* **516**, 465.
Filippov, B. P.: 1995, *Astron. Astrophys.* **303**, 242.
Finn, J. M. and Chen, J.: *Astrophys. J.* **349**, 345.
Finn, J. M., Guzdar, P. N. and Chen, J.: 1992, *Astrophys. J.* **393**, 800.
Fisher, R. R. and Munro, R. H.: 1984, *Astrophys. J.* **280**, 428.
Fisher, R. R., Lee, R. H., MacQueen, R. M. and Poland, A. I.: 1981, *Appl. Optics* **20**, 1094.
Forbes, T. G. and Priest, E. R.: 1995, *Astrophys. J.* **446**, 377.
Garren, D. A. and Chen, J.: 1994, *Phys. Plasmas* **1**, 3425.
Gold, T. and Hoyle, F.: 1960, *Mon. Notices Royal Astron. Soc.* **120**, 89.
Gosling, J. T.: 1990, in C. T. Russell, E. R. Priest, and L. C. Lee (eds), *Physics of Magnetic Flux Ropes*, *Geophys. Monogr.*, vol. 58, eds. AGU, Washington, D.C., p. 343.
Gosling, J. T.: 1993, *J. Geophys. Res.*, **98**, 18937.
Gosling, J. T.: 1999, *Magnetic Helicity in Space and Laboratory Plasmas*, Geophys. Monogr. 111, AGU, Washington, D.C., p. 205.
Gosling, J. T., Hildner, E., MacQueen, R. M., Munro, R. H., Poland, A. I. and Ross, C. L.: 1974, *J. Geophys. Res.* **79**, 4581.
Gosling, J. T., McComas, D. J., Phillips, J. L. and Bame, S. J.: 1991, *J. Geophys. Res.* **96**, 7831.
Hénoux, J. C. and Somov, B. V.: 1987, *Astron. Astrophys.* **185**, 306.
Heyvaerts, J.: 1974, *Solar Phys.* **38**, 419.
Heyvaerts, J., Priest, E. R. and Rust, D. M.: *Astrophys. J.* **216**, 123.
Heyvaerts, J., Lasry, J. M., Schatzman, M. and Witomsky, P.: 1982, *Astron. Astrophys.* **111**, 104.
Hodgson, R.: 1860, *Monthly Notices Royal Astron. Soc.* **20**, 16.
Hood, A. W. and Priest, E. R.: 1979, *Solar Phys.* **64**, 303.
Howard, R. A., Michels, D. J., Sheeley, N. R., Jr. and Koomen, M. J.: 1982, *Astrophys. J.* **263**, L101.
Howard, R. A., Sheeley, N. R., Jr., Koomen, M. J. and Michels, D. J.: 1985, *J. Geophys. Res.* **90**, 8173.
Huba, J. D. and Chen, J.: 1996, *Astrophys. J.* **469**, 412.
Hundhausen, A. J.: *J. Geophys. Res.* **98**, 13177.
Hundhausen, A. J., Burkepile, J. T. and St. Cyr, O. C.: 1994, *J. Geophys. Res.* **99**, 6543.
Hundhausen, A. J.: 1999, in K. Strong, J. Saba, B. Haisch, and J. Schmelz (eds), *The Many Faces of the Sun*, Springer-Verlag, New York, p. 143.
Illing, R. M. E. and Hundhausen, A. J.: 1983, *J. Geophys. Res.* **88**, 10210.
Illing, R. M. E. and Hundhausen, A. J.: 1986, *J. Geophys. Res.* **91**, 10951.

Jockers, K.: 1978, *Solar Phys.* **56**, 37.
Kahler, S. W.: 1992, *Ann. Rev. Astron. Astrophys.* **30**, 113.
Kan, J. R., Akasofu, S.-I. and Lee, L.-C.: 1983, *Solar Phys.* **84**, 153.
Klimchuk, J. A. and Sturrock, P. A.: 1989, *Astrophys. J.* **345**, 1034.
Krall, J., Chen, J. and Santoro, R.: 2000, *Astrophys. J.* (in press).
Kumar, A. and Rust, D. M.: 1996, *J. Geophys. Res.* **101**, 15667.
Kuperus, M. and Raadu, M. A.: 1974, *Astron. Astrophys.* **31**, 189.
Larson, E. E., *et al.*: 1997, *Geophys. Res. Lett.* **24**, 1911.
Leka, K. D., Canfield, R. C., McClymont, A. N. and van Driel-Gesztelyi, L.: 1996, *Astrophys. J.* **462**, 547.
Lepping, R. P., Jones, J. A. and Burlaga, L. F.: 1990, *J. Geophys. Res.* **95**, 11957.
Lionello, R., Velli, M., Einaudi, G. and Mikić, Z.: 1998, *Astrophys. J.* **494**, 840.
Lites, B. W., Low, B. C., Martínez Pillet, V., Seagraves, P., Skumanich, A., Frank, Z. A., Shine, R. A. and Tsuneta, S.: 1995, *Astrophys. J.* **446**, 877.
Low, B. C.: 1977, *Astrophys. J.* **212**, 234.
Low, B. C. and Hundhausen, J. R.: 1995, *Astrophys. J.* **443**, 818.
McClymont, A. N. and Fisher, G. H.: 1989, *Geophys. Mongr.* AGU, p. 219.
McComas, D. J., Phillips, J. L., Hundhausen, A. J. and Burkepile, J. T.: 1991, *Geophys. Res. Lett.* **18**, 73.
MacQueen, R. M., Eddy, J. A., Gosling, J. T., Hildner, E., Munro, R. H., Newkirk, G. A., Poland, A. I., and Ross, C. L.: 1974, *Astrophysical J.* **187**, L85.
MacQueen, R. M., Csoeke-Poeckh, A., Hildner, E., House, L., Reynolds, R., Stanger, A., Tepoel, H. and Wagner, W.: 1980, *Solar Phys.* **65**, 91.
MacQueen, R. M. and Fisher, R. R.: 1982, *Astrophys. J.* **254**, 335.
Melrose, D. B. and Khan, J. I.: 1989, *Astron. Astrophys.* **219**, 308.
Melrose, D. B. and McClymont, A. N.: 1987, *Solar Phys.* **113**, 241.
Michels, D. J., Howard, R. A., Koomen, M. J. and Sheeley, N. R. Jr.: 1980, in M. Dryer and E. Tandberg-Hanssen (eds.), *Solar and Interplanetary Dynamics* p. 387.
Mikić, Z. and Linker, J. A.: 1994, *Astrophys. J.* **430**, 898.
Mikić, Z., Barnes, D. C. and Schnack, D. D.: 1988, *Astrophys. J.* **328**, 830.
Moore, R. L., *et al.*: 1980, in P. A. Sturrock (ed.), *Solar Flares*, Colorado Associated University Press, Boulder, Chapter 8, p. 341.
Mouschovias, T. C. and Poland, A. I.: 1978, *Astrophys. J.* **220**, 675.
Munro, R. H., Gosling, J. T., Hildner, E., MacQueen, R. M., Poland, A. I. and Ross, C. L.: 1979, *Solar Phys.* **61**, 201.
Parker, E. N.: 1996, *J. Geophys. Res.* **101**, 10587.
Poland, A. I., Howard, R. A., Koomen, M. J., Michels, D. J. and Sheeley, N. R., Jr.: 1981, *Solar Phys.* **69**, 169.
Rompolt, B.: 1975, *Solar Phys.* **41**, 329.
Russell, C. T., McPherron, R. L. and Burton, R. K.: 1974, *J. Geophys. Res.* **79**, 1105.
Rust, D. M.: 1967, *Astrophys. J.* **150**, 313.
Rust, D. M.: 1972, *Solar Phys.* **25**, 141.
Rust, D. M.: 1994, *Geophys. Res. Lett.* **21**, 241.
Schmahl, E. and Hildner, E.: 1977, *Solar Phys.* **55**, 473.
Schrijver, C. J., *et al.*: 1999, *Solar Phys.* **187**, 261.
Sen, H. K. and White, M. L.: 1972, *Solar Phys.* **23**, 146.
Shay, M. A., Drake, J. F., Rogers, B. N. and Denton, R. E.: 1999, *Geophys. Res. Lett.* **26**, 2163.
Sheeley, N. R. Jr., Howard, R. A., Koomen, M. J., Michels, D. J., Harvey, K. L. and Harvey, J. W.: 1982, *Space Sci. Rev.* **33**, 219.
St. Cyr, O. C., Burkepile, J. T., Hundhausen, A. J. and Lecinski, A. R.: 1999, *J. Geophys. Res.* **104**, 12493.

Sturrock, P. A.: 1980, in P. A. Sturrock (ed.), *Solar Flares*, Colorado Associated University Press, Boulder, Chapter 9, p. 411.
Sturrock, P. A.: 1991, *Astrophys. J.* **380**, 655.
Svestka, Z.: 1976, *Solar Flares*, D. Reidel Publ. Co., Dordrecht, The Netherlands.
Tanaka, K.: 1991, *Solar Phys.* **136**, 133.
Tandberg-Hanssen, E.: 1995, *The Nature of Solar Prominences*, Kluwer Academic Publishers, Dordrecht, The Netherlands.
Tousey, R.: 1973, *Space Res.* **13**, 713.
Vršnak, B., Ruždjak, V. and Rompolt, B.: 1991, *Solar Phys.* **136**, 151.
Wang, H., Ewell, M. W., Jr., and Zirin, H.: 1994, *Astrophys. J.*, **424**, 436.
Webb, D. F.: 1988, *J. Geophys. Res.* **93**, 1749.
Webb, D. F. and Cliver, E. W.: 1995, *J. Geophys. Res.* **100**, 5853.
Webb, D. F., Cliver, E. W., Crooker, N. U., St. Cyr, O. C. and Thompson, B. J.: 2000, *J. Geophys. Res.* **105**, 7491.
Wilson, R. M. and Hildner, E.: 1984, *Solar Phys.* **91**, 169.
Wolfson, R. and Low, B. C.: 1992, *Astrophys. J.* **391**, 353.
Wolfson, R. and Saran, S.: 1998, *Astrophys. J.* **499**, 496.
Wood, B. E., Karovska, M., Chen, J., Brueckner, G. E., Cook, J. W. and Howard, R. A.: 1999, *Astrophys. J.* **512**, 484.
Wu, S. T., Guo, W. P. and Dryer, M.: 1997, *Solar Phys.* **170**, 265.
Wu, S. T., *et al.*: 1997, *Solar Phys.* **175**, 719.
Wu, S. T., Guo, W. P., Michels, D. J. and Burlaga, L. F.: 1999, *J. Geophys. Res.* **104**, 14789.
Xue, M. L. and Chen, J.: 1983, *Solar Phys.* **84**, 119.
Zweibel, E. G. and Boozer, A. H.: 1985, *Astrophys. J.* **295**, 642.
Zhang, G. and Burlaga, L. F.: 1988, *J. Geophys. Res.* **93**, 2511.
Zwingmann, W.: 1987, *Solar Phys.* **111**, 309.